Oil & Gas Science and Technology – Rev. IFP, Vol. 54 (1999), No. 2, pp. 233-244

3D Simulation of DI Diesel Combustion and Pollutant Formation Using a Two-Component Reference Fuel

H. Barths[1], H. Pitsch[1] and N. Peters[1]

1 Institut für Technische Mechanik, RWTH Aachen, Templergrassen 64, 52056 Aachen - Germany
e-mail: h.barths@itm.rwth-aachen.de - n.peters@itm.rwth-aachen.de

Résumé — Simulation 3D de la combustion et de la formation des polluants dans un moteur Diesel à injection directe en utilisant un carburant de référence à deux composants — En séparant calculs aérodynamiques et calculs chimiques, le modèle instationnaire de « flamelet » permet d'introduire des mécanismes chimiques complets qui comprennent plusieurs centaines de réactions. Ceci est indispensable pour décrire les différents processus qui ont lieu dans un moteur Diesel à injection directe (ID) tels que l'auto-inflammation, la fin de la phase de prémélange partiel, la transition vers une combustion diffusive et la formation de polluants tels que les NO_x et les suies. Il n'est pas nécessaire de simplifier les taux de réactions hautement non linéaires, d'autre part, la structure complète du processus de combustion est conservée.

En utilisant le modèle de type « Representative Interaction Flamelet » (RIF), l'ensemble monodimensionnel instationnaire d'équations différentielles aux dérivées partielles est résolu en interaction avec le code CFD 3D. La solution ainsi obtenue est couplée avec les flux gazeux et le champ de mélange par l'intermédiaire de plusieurs paramètres dépendant du temps (l'enthalpie, la pression, le taux scalaire de dissipation). En retour, le modèle de « flamelet » fournit les concentrations moyennes des espèces chimiques, qui sont ensuite exploitées par le code CFD 3D pour calculer les champs de températures et les densités. La densité est nécessaire au code CFD 3D pour déterminer les flux turbulents et le champ de mélange.

La formation des polluants est déterminée expérimentalement dans un moteur Diesel Volkswagen DI 1900. Le moteur est alimenté avec du gazole et deux carburants de référence. Un des carburants de référence est du *n*-décane pur. Le second est un carburant bicomposant formé de 70 % (du volume liquide) de *n*-décane et de 30 % d'α-méthylnaphtalène *(Idea-fuel)*. Les résultats expérimentaux indiquent un bon accord sur toute la phase de combustion (délai d'allumage, pression maximale, couple et formation des polluants) entre le carburant de référence bicomposant et le gazole. Les simulations sont réalisées pour les deux carburants de référence et sont comparées aux données expérimentales. Neuf calculs de « flamelet » différents sont effectués pour chaque simulation de manière à prendre en compte la variabilité du taux scalaire de dissipation dont les effets sur le déclenchement de la combustion sont ici commentés. Nous établissons la formation des polluants (NO_x et suies) pour les deux carburants de référence. La contribution des différents mécanismes de réactions pour la formation du NO est indiquée (thermique, prompt, protoxyde, recombustion). Enfin, nous dressons un examen de l'importance du processus de mélange pour la prévision des suies.

Mots-clés : moteur Diesel, polluants.

Abstract*—*3D Simulation of DI Diesel Combustion and Pollutant Formation Using a Two-Component Reference Fuel *— By separating the fluid dynamic calculation from that of the chemistry, the unsteady flamelet model allows the use of comprehensive chemical mechanisms, which include several hundred reactions. This is necessary to describe the different processes that occur in a DI Diesel engine such as autoignition, the burnout in the partially premixed phase, the transition to diffusive burning, and formation of pollutants like NO_x and soot. The highly nonlinear reaction rates need not to be simplified, and the complete structure of the combustion process is preserved.*

Using the Representative Interactive Flamelet (RIF) model the one-dimensional unsteady set of partial differential equations is solved online with the 3D CFD code. The flamelet solution is coupled to the flow and mixture field by several time dependent parameters (enthalpy, pressure, scalar dissipation rate). In return, the flamelet code yields the species concentrations, which are then used by the 3D CFD code to compute the temperature field and the density. The density is needed in the 3D CFD code for the solution of the turbulent flow and mixture field.

Pollutant formation in a Volkswagen DI 1900 Diesel engine is investigated experimentally. The engine is fueled with Diesel and two reference fuels. One reference fuel is pure n*-decane. The second is a two-component fuel consisting of 70% (liquid volume)* n*-decane and of 30% (liquid volume) α-methylnaphthalene* (Idea-fuel). *The experimental results show good agreement for the whole combustion cycle (ignition delay, maximum pressures, torque and pollutant formation) between the two-component reference fuel and Diesel. The simulations are performed for both reference fuels and are compared to the experimental data. Nine different flamelet calculations are performed for each simulation to account for the variability of the scalar dissipation rate, and its effect on ignition is discussed. Pollutant formation (NO_x and soot) is predicted for both reference fuels. The contributions of the different reaction paths (thermal, prompt, nitrous, and reburn) to the NO formation are shown. Finally, the importance of the mixing process for the prediction of soot emissions is discussed.*

Keywords: Diesel engine, pollutant.

INTRODUCTION

The physical and chemical complexity of Diesel-fuel considering its many compounds imposes insurmountable problems to the modeler. As a remedy reference fuels are considered, for which chemical reaction mechanisms have been developed. Diesel and Idea-fuel (70% (liquid volume) *n*-decane and 30% (liquid volume) α-methyl-naphthalene) show good agreement in their physical (density, viscosity, etc.) and chemical (cetane number, aliphatic and aromatic compounds) similarity. This Idea-fuel and a second reference fuel (pure *n*-decane) are compared to Diesel experimentally in a Volkswagen DI Diesel engine at different loads.

Simulations with the two reference fuels were performed applying the "Representative Interactive Flamelet" (RIF) model is rigorously derived from the equations governing the physics of combustion [1] and does therefore not require the tuning of parameters. Since it is based on the flamelet approach, it allows the application of detailed chemistry. Hence, auto-ignition, partially premixed burning, diffusive combustion and pollutant formation need not to be modeled separately, but are part of the comprehensive chemical mechanism, which consists of 118 species and 557 elementary reactions including fuel oxidation, and low temperature degenerate chain branching to describe auto-ignition. It also comprises a reaction mechanism for NO_x formation including thermal (Zel'dovic), prompt, nitrous NO, and reburn by hydrocarbon radicals and a detailed description of benzene and polycylic aromatic hydrocarbon (PAH) formation as part of the soot model.

This model was already applied to the simulation of a combustion bomb and a *n*-heptane fueled Diesel engine [2, 3]. Recently, the RIF concept was extended to multiple flamelets. The effects of multiple flamelets on the combustion process is investigated and the computational results are compared to the experimental data for *n*-decane and Idea-fuel.

1 RIF MODEL

Flamelet modeling has the advantage of separating the numerical effort associated with the resolution of small chemical time and length scales from the CFD-computation of the engine combustion cycle [4]. Concluding from the to eddy dissipation models analogous assumption that the chemical time and length scales are much smaller than the turbulent ones, follows that the flame sheet can merely be stretched and distorted by the smallest turbulent eddies. Therefore, the laminar flame structure is disturbed locally, but preserved. Introducing a conserved scalar *Z*, which is the mixture fraction, defined by the transport equation:

$$\rho \frac{\partial Z}{\partial t} + \rho v_\alpha \frac{\partial Z}{\partial x_\alpha} - \frac{\partial}{\partial x_\alpha}\left(\rho D_Z \frac{\partial Z}{\partial x_\alpha}\right) = 0 \qquad (1)$$

with the boundary conditions $Z = 1$ in the pure fuel stream and $Z = 0$ in pure oxidizer stream one can show that the gradient of Z is perpendicular to the flame sheet. The diffusion coefficient D_Z in Equation (1) can be defined arbitrarily and was set such that the Lewis-number Le_Z is equal to one. Considering a locally defined coordinate system, where one coordinate x_1 is Z and thereby perpendicular to the flame sheet and the other two x_2, x_3 lie within the flame sheet, the conservation equations for the species and temperature can be transformed. After an order of magnitude analysis of the terms of the resulting equations and the neglect of the terms, which are small to leading order, the equations appear in one-dimensional form [1, 5].

These are the so called flamelet equations:

$$\rho \frac{\partial T}{\partial t} - \rho \frac{\chi}{2} \frac{\partial^2 T}{\partial Z^2} - \rho \frac{\chi}{2c_p} \frac{\partial T}{\partial Z} \frac{\partial c_p}{\partial Z} - \sum_i^N \rho \frac{\chi}{2Le_i} \frac{c_{pi}}{c_p} \frac{\partial Y_i}{\partial Z} \frac{\partial T}{\partial Z} + \frac{1}{c_p} \sum_i^N \dot{m}_i h_i - \frac{1}{c_p} \frac{\partial p}{\partial t} = 0 \quad (2)$$

and:

$$\rho \frac{\partial Y_i}{\partial t} - \rho \frac{\chi}{2Le_i} \frac{\partial^2 Y_i}{\partial Z^2} - \dot{m}_i + \frac{1}{2} \left[\rho\chi \frac{1}{Le_i^2} \frac{\partial Le_i}{\partial Z} + \frac{1}{2} \left(1 - \frac{1}{Le_i}\right) \left(\frac{\partial \rho\chi}{\partial Z} + \rho\chi \frac{c_p}{\lambda} \frac{\partial}{\partial Z} \left(\frac{\lambda}{c_p} \right) \right) \right] \frac{\partial Y_i}{\partial Z} = 0 \quad (3)$$

In these equations N denotes the number of chemical species, p the pressure, c_{pi}, $\dot{m}_i$, h_i, and Y_i are the heat capacities at constant pressure, the chemical production rates, the enthalpies, and the mass fractions of the chemical species i, respectively.

The Lewis-numbers in Equations (2) and (3) are defined by:

$$Le_i = \frac{\lambda}{\rho D_i c_p} \quad (4)$$

In Equations (2) and (3), no convective terms appear. This is due to the fact, that all scalars, e.g. Z, T, Y_i, are transported with the same convection velocity. In Equation (3) however, the last term, accounting for the differential diffusion in mixture fraction space, may also be interpreted as convective term [6]. The influence of the flow field is now represented by the scalar dissipation rate:

$$\chi = 2D_Z \left(\frac{\partial Z}{\partial x_k} \right)^2 \quad (5)$$

which is a crucial parameter in flamelet modeling accounting for strain effects. Further parameters, which influence the flamelet solution, are the pressure and the boundary conditions. These are discussed in the following.

The history of the flamelet parameters is important for the solution of the flamelets, which consequently have to be solved unsteadily. This leads to the RIF concept. The flamelet equations are solved in a separate code, interactively coupled with a CFD code. Each time step the CFD code solves its own set of equations, it also makes a call to the flamelet code, which solves the unsteady flamelet equations with time steps that can be much smaller, e.g. during ignition. In this way the time scales of the fluid dynamics and the chemistry are decoupled.

The interaction between the CFD code and the flamelet code is shown schematically in Figure 1.

The coupling between the CFD code and the flamelet code is established by extracting the flamelet parameters from the CFD code by statistically averaging over the representative flamelet domain.

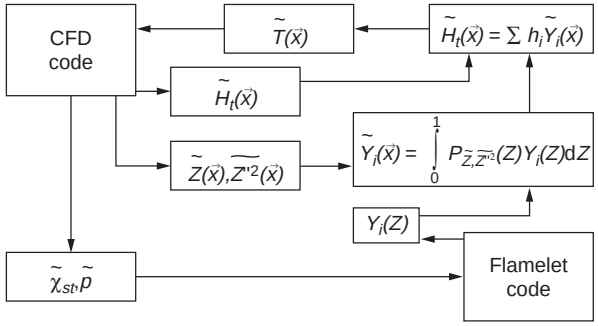

Figure 1

Code structure of Representative Interactive Flamelet (RIF) concept.

Vice versa, the coupling between the flamelet code and the CFD code is obtained by computing the local temperature $\tilde{T}$ in the CFD code from the local enthalpy $\tilde{H}$ and the species mass fractions Y_i extracted from the flamelet solution via the identity:

$$\widetilde{H} = \sum_{i=1}^{N} \widetilde{Y}_i \, h_i \, (\widetilde{T}) \quad (6)$$

The mean species mass fractions $\widetilde{Y}_i$ in Equation (6) are computed by integrating the current flamelet solution weighted with a presumed probability density function (PDF):

$$\widetilde{Y}_i(\vec{x}) = \int_0^1 P_{\widetilde{Z},\widetilde{Z''^2}}(Z) Y_i(Z) \, \mathrm{d}Z \quad (7)$$

The beta-PDF $P_{\widetilde{Z},\widetilde{Z''^2}}(Z)$ employed here is a function of Z only, but its shape is determined by two parameters, which are the local mean mixture fraction $\widetilde{Z}$ and its variance ($\widetilde{Z''^2}$). Hence, the mean species mass fractions also depend on the local values of $\widetilde{Z}$ and ($\widetilde{Z''^2}$) only, and although the same flamelet solution is used for different locations different mean species mass fractions are obtained. The beta-PDF has been shown to be a good approximation for turbulent jets [7].

1.1 Multiple Flamelets

The unsteady flamelet equations represent a parabolic set of coupled partially differential equations. Hence, the flamelet solution is defined by the initial and boundary conditions, and by the time-dependent scalar dissipation rate. In most technical applications like gas turbine combustors and Diesel engines the initial conditions do not vary in space. Under the assumption that the composition of the fuel and oxidizer stream do not vary in time, the boundary conditions for the species conservation equations remain constant, also.

The scalar dissipation rate additionally varies in space within the combustion chamber. Thus, mass particles with initially different locations will experience a different history for the scalar dissipation rate.

Hence, a concept for multiple flamelets must account for:
- the spatially varying scalar dissipation rate and
- must relate the history of the scalar dissipation rate to mass particles in the flow field;
- an additional requirement is the independence of the concept from the geometry of the problem.

The tracking of the mass weighted fraction of particles corresponding to the flamelet l is achieved by solving a marker equation for each particle (flamelet) which has the following form for a laminar flow field (neglecting diffusion):

$$\frac{\partial \rho I_l}{\partial t} + \nabla \cdot (\rho\, I_l\, \vec{v}) = 0 \tag{8}$$

with ρ denoting the density, I_l the mass fraction of particle l among the total number of particles, and $\vec{v}$ the velocity vector. In a turbulent flow field this advection equation converts to a convection-diffusion equation due to the turbulent diffusion:

$$\frac{\partial \bar{\rho}\tilde{I}_l}{\partial t} + \nabla \cdot (\bar{\rho}\, \tilde{I}_l\, \vec{\tilde{v}}) - \nabla \cdot \left(\bar{\rho}\, \frac{\nu_T}{Sc_l}\, \nabla \tilde{I}_l\right) = 0 \tag{9}$$

where the bar denotes ensemble averaging and the tilde denotes Favre ensemble averaging. The coefficient ν_T is the turbulent viscosity and Sc_l is the turbulent Schmidt number.

Note that due to the turbulent mixing process several particles can be found at the same location. Therefore, the expected value of the occurrence of a particle $\tilde{I}_l$ will be smaller than one, but:

$$\sum_{l=1}^{n_l} \tilde{I}_l = 1 \tag{10}$$

will hold everywhere. Here n_l represents the total number of different particles present in the computation.

The Z-dependence of the scalar dissipation rate χ as taken from [1]:

$$\chi\,(Z) = \frac{a}{\pi} \exp\left\{-2\left[\mathrm{erfc}^{-1}(2Z)\right]^2\right\} \tag{11}$$

This can be expressed as:

$$\chi\,(Z, \vec{x}) = \frac{\chi_{st}\,(\vec{x})}{f(Z_{st})}\, f(Z) \tag{12}$$

which is modelled as:

$$\tilde{\chi} = c_\chi \frac{\tilde{\varepsilon}}{\tilde{k}} \widetilde{Z''^2} \tag{13}$$

where $c_\chi = 2.0$. A surface averaged value for the scalar dissipation rate at stoichiometric mixture for each flamelet is computed following Pitsch [8] by converting the surface integrals into volume integrals. Here it is weighted additionally with the expected value of the occurrence of particle l:

$$\widehat{\chi_{st}}(l) = \frac{\int_V \tilde{I}_l\,(\vec{x})\, \bar{\rho}(\vec{x})\, \chi_{st}^{3/2}(\vec{x})\, p\; \mathrm{d}f(Z_{st})\, \mathrm{d}V'}{\int_V \tilde{I}_l\,(\vec{x})\, \bar{\rho}(\vec{x})\, \chi_{st}^{1/2}(\vec{x})\, p\; \mathrm{d}f(Z_{st})\, \mathrm{d}V'} \tag{14}$$

In order to determine the number n_l of different particles that are needed for the computations, we determine how much the scalar dissipation rates for each of the different particles vary. Each particle covers only a specific range in the distribution of the scalar dissipation rate and is thereby defined. The variance of the scalar dissipation rate is a measure for the inhomogeneity of the distribution of the scalar dissipation rate in a particle. If the variance of the scalar dissipation rate, calculated from its distribution within a particle, exceeds a certain limit, this particle must be subdivided corresponding to the level of the scalar dissipation rate.

1.2 CFD Code

For each flamelet a particle equation of the type of Equation (9) has to be solved in the CFD code, which in this case is a modified version of the TurboKiva code. Since these equations are of a simple convection-diffusion type, their solution does not result in a significant penalty in computational cost.

In addition two transport equations for the mixture fraction ($\tilde{Z}$) and the mixture fraction variance ($\widetilde{Z''^2}$) have to be solved in the CFD code to define the local mean species composition:

$$\frac{\partial(\bar{\rho}\tilde{Z})}{\partial t} + \nabla \cdot (\bar{\rho}\, \vec{u}\, \tilde{Z}) = \nabla \cdot \left[\frac{\mu}{Sc_{\tilde{Z}}} \nabla \tilde{Z}\right] + \dot{\rho}^s \tag{15}$$

$$\frac{\partial(\bar{\rho}\widetilde{Z''^2})}{\partial t} + \nabla \cdot (\bar{\rho}\, \vec{u}\, \widetilde{Z''^2}) = \nabla \cdot \left[\frac{\mu}{Sc_{\widetilde{Z''^2}}} \nabla \widetilde{Z''^2}\right] + \frac{2\mu}{Sc_{\widetilde{Z''^2}}} (\nabla \tilde{Z})^2 - \bar{\rho}\, \tilde{\chi} \tag{16}$$

One more change to the original TurboKiva code was made. In order to avoid the chemical source term in the conservation equation for the internal energy, the formulation was altered to the total enthalpy:

$$H = \Delta h_f^o + \int_{T^o}^{T} c_p\, \mathrm{d}T \tag{17}$$

which includes the chemical heat of formation of the species Δh_f^o.

$$\frac{\partial(\bar{\rho}\tilde{H})}{\partial t} + \nabla \cdot (\bar{\rho}\, \vec{u}\, \tilde{H}) = \frac{D\tilde{p}}{Dt} - \nabla \cdot \vec{J} + \bar{\rho}\, \tilde{\varepsilon} + \dot{Q}^s \tag{18}$$

In these equations, the heat flux vector $\vec{J}$ is the sum of the contributions from heat conduction and enthalpy flux term. $\dot{Q}^s$ and $\dot{\rho}^s$ represent the heat and mass transfer from droplets to the gaseous phase, and are determined by the spray model. $Sc_{\tilde{Z}}$ and $Sc_{\widetilde{Z''^2}}$ are constants. For the present study a value of 0.9 was chosen for both. All other models are described in [9].

1.3 Chemistry Model

The complete chemical reaction mechanism comprises 557 elementary reactions and 118 chemical species. This mechanism describes low and high temperature auto-ignition, fuel decomposition, and fuel oxidation, as well as formation of soot precursors and NO_x. The *n*-decane mechanism was taken from Pitsch [10]. The $C_1 - C_2$ and the O/H chemistry mainly has been taken from Baulch *et al.* [11]. Low temperature kinetic rate data have been taken from Benson [12] and Chevalier *et al.* [13]. The rates for external as well as internal H-abstraction reactions from fuel and from species, which are involved in the low temperature chemistry have been calculated following Westbrook *et al.* [14]. The NO_x submechanism taken from Hewson *et al.* [15] accounts for thermal, prompt, and nitrous oxide contributions to NO_x formation, and for NO_x reburn by hydrocarbon radicals and amines (NH_x). Soot precursor chemistry is described up to benzene via the C_3-, as well as via the C_4- chain, following Mauss [16] based on Frenklach *et al.* [17] and Miller *et al.* [18] and simplified by Pitsch [19]. Further formation and growth of small polycyclic aromatic hydrocarbons (PAHs) is included in the mechanism up to PAHs consisting of four aromatic rings.

The formation, the growth, and the oxidation of soot particles is described by a kinetically based model. A method using statistical moments is employed [16, 20]. For the present study only the equations for the first two statistical moments are solved, which can physically be interpreted as the particle number density of soot particles and the number density of the smallest counted mass units representing the soot volume fraction. The soot model accounts for particle inception due to PAH coagulation, condensation of PAHs on the soot particle surface, coagulation of soot particles, and heterogeneous surface reactions, leading globally to soot mass growth by acetylene addition and particle oxidation by OH and molecular oxygen attack.

2 EXPERIMENTS

The experiments were performed with the Volkswagen transparent DI 1900 Diesel engine. The transparent engine was experimentally investigated during the Idea and the Idea-Effect program by Arcoumanis *et al.* [21], Bäcker *et al.* [22], and Hentschel *et al.* [23-25]. In contrast to this previous experiments the mexican hat shaped piston bowl of the production engine was inserted in the piston instead of the quartz glass window. The decreased stiffness of the extended piston, which was constructed for the optical access through the piston bowl, reduced the compression ratio to 17.5:1. The pollutant concentrations (and soot) in the exhaust gas were measured by Antoni [26] and Douch [27]. The exhaust gas analysis was carried out using standard exhaust instrumentation and a heated gas probing valve and line positioned just downstream of the exhaust valve. The soot probing technique was the Bosch method applying a Bosch smoke meter and NO_x-probing was carried out with a chemiluminescence analyzer (CLD).

For the thermodynamic measurements of the in-cylinder pressure a standard water-cooled piezo-electric pressure transducer (Kistler 601, sensitivity 16 pC/bar) was used, which was mounted instead of a piston side window. At top dead center this location is in the crevice region. Due to this positioning the measured pressure traces are disturbed by pipe oscillations.

The intake air mass flow rates were jointly measured for all four cylinders with a hot film anemometer (Deguflow 8740-20 300, range < 400 kg/h). Pulsations from the intake manifold were compensated with a damping tube.

The injection system consisted of a Bosch VP37 pump and a one spring five hole nozzle with a nozzle diameter of 0.184 mm. The injection rates were measured with a Bosch-tube with *n*-decane by Wolter [28] and are shown in Figure 2. Each rate represents the average of 50 cycles. They show a linear increase of the injection duration with increasing injection volume.

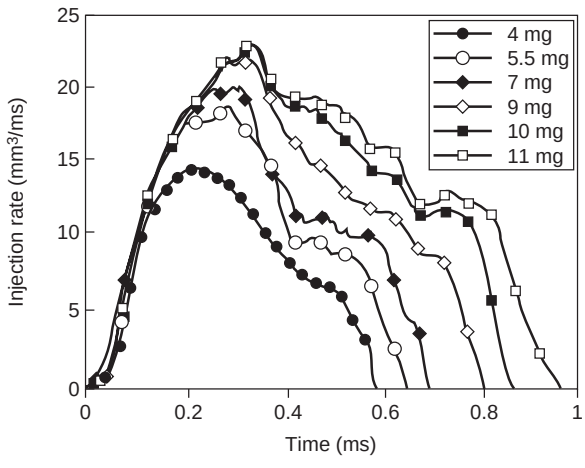

Figure 2

Measured injection rates (*n*-decane).

The engine was fueled with three different fuels: two model fuels, and Diesel. The first model fuel was pure *n*-decane. Due to the reduced lubrication and the lower density of *n*-decane compared to Diesel fuel, the fuel mass of

11 mg per injection was the maximum the injection pump was able to supply without damage.

The second model fuel was a mixture of *n*-decane and α-methylnaphthalene. The liquid mixture consisted of 70% (volume) *n*-decane and 30% (volume) α-methylnaphthalene. It was thoroughly investigated in the Idea-Effect program and will be called Idea-fuel in the following. The physical and chemical properties of the Idea-fuel and Diesel are very similar. The densities at standard conditions are 817 kg/m^3 for the Idea-fuel and 840 kg/m^3 for Diesel compared to 730 kg/m^3 for *n*-decane. The cetane number for Diesel is 53 and 56 for the Idea fuel.

This similarity results in an almost identical behavior of both fuels concerning vaporization, ignition, and heat release. This is shown in Figure 3, where the measured cylinder pressures are plotted versus crank angle (CA) for both fuels. The start of injection is 11° CA before top dead center (BTDC). The injected fuel mass is 16 mg. The pressure traces are hardly to distinguish, and thereby, proving the similarity.

Figures 4 and 5 show the dependence of the pollutant formation on injected fuel mass for all three fuels. In these figures the exhaust gas values are plotted versus torque rather than injected fuel mass, since the injected fuel mass was not measured online with the experiments, but the torque was. The start of injection (SOI) was at 11° CA BTDC for Diesel and Idea, and 8° CA BTDC for *n*-decane. In all cases ignition occurred at TDC. Figure 4 reveals an almost linear increase of the NO_x concentration in the exhaust gas with increasing torque. The gradient for Diesel and Idea is the same, with slightly higher absolute values for Diesel (difference 3-7%). Both values are lower for *n*-decane. It produces approximately 30% less NO_x than Diesel.

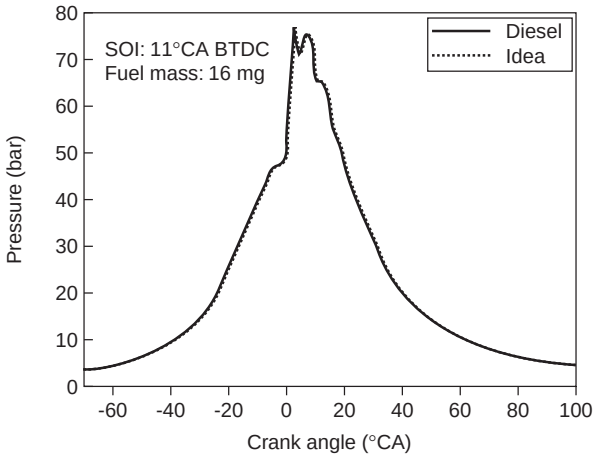

Figure 3

Comparison of the pressures obtained for Diesel and Idea-fuel.

The soot mass concentration increases approximately exponentially with increasing torque for Diesel and Idea, as displayed in Figure 5. In the range of the torque between 40-80 Nm Idea produces 30% less soot than Diesel, whereas the deviation for higher and lower loads is around only 10%. For *n*-decane soot shows only a linear dependence and only an absolute amount of 30% of soot is produced compared to diesel. The difference in the soot production is probably due to the fact that *n*-decane does not contain aromatic compounds, which are important as soot precursors for the formation of soot.

Overall, good agreement is found between Idea and Diesel, qualitatively as well as quantitatively.

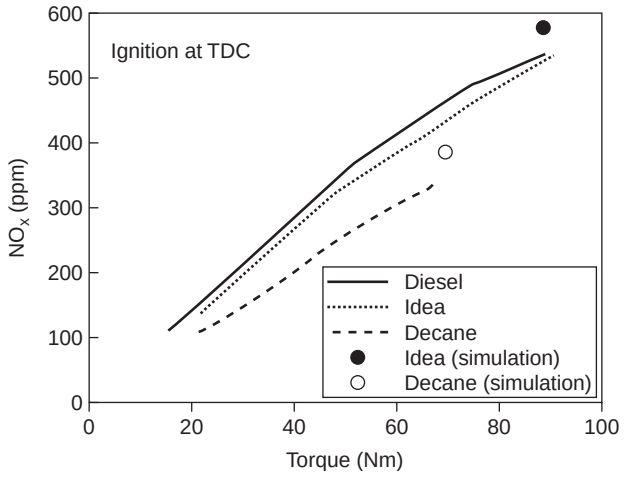

Figure 4

Exhaust gas values of NO_x for different fuels and loads.

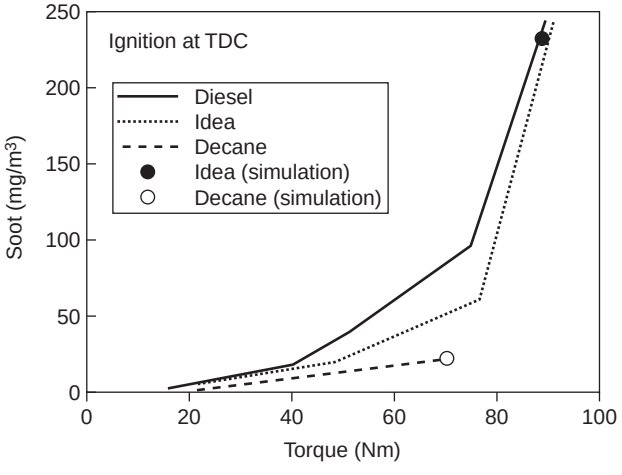

Figure 5

Exhaust gas values of soot for different fuels and loads.

3 NUMERICAL RESULTS

The computations were performed for *n*-decane (7 and 11 mg, SOI 8° CA BTDC) and Idea-fuel (16 mg, SOI 11° CA BTDC). The computations started at 70 degrees crank angle BTDC and ended 100 degrees after top dead center (ATDC) at the point where the exhaust valve opens. The average cylinder pressure and temperature at the beginning of the calculation were taken from previous calculations by Strauss [29] including the intake valve. This calculations again started from experimentally obtained data by Arcoumanis *et al.* [30]. The wall temperatures were set such that pressures matched for the compression phase before injection started. They were held constant during the computations. The swirl was set to 2.5 times the number of revolutions of the engine (tr/min) in correspondence to the measured swirl. Although the injection nozzle was located slightly off the axis of symmetry due to the different sizes of the intake and exhaust valves in the engine, only a sector of 72° with periodic boundaries was simulated in favor of computational resources. The number of grid cells at TDC was 20 in radial, 24 in azimuthal, and 10 in axial direction. The applied mesh resolution proved to give reasonable results in previous simulations [3, 31].

The influence of the number of flamelets on heat release and pressure is investigated in Figure 6. For the case of 7 mg injected fuel mass with start of injection at 8° CA only the number of flamelets was changed (1, 9 and 20 flamelets) in the simulations. The simulation with one flamelet shows a very strong heat release right after ignition occurs resulting in a strong pressure rise. This is due to the fact that all the mixture that is close to stoichiometric ignites at once. In the case with 20 flamelets each flamelet has its own history and, hence, an individual level of the scalar dissipation rate. Thus, the flamelets ignite consecutively. The heat release in the so called partially premixed phase of the combustion is more moderate, and the pressure is almost identical with the measured curve. Only in the very early and the late partially premixed phase the heat release slightly deviates in the simulation.

The very rapid heat release in the case with one flamelet leads to a likewise strong expansion. As a consequence the turbulence intensity k rises stronger than in the more realistic case with 20 flamelets. This is documented in Figure 7, which shows the cylinder averaged values for the turbulence intensity. The first increase of the turbulence intensity is generated by the injected fuel. In contrast the turbulent integral length scale L remains the same in both cases. Since the turbulent viscosity is defined by $\nu = Lk^{0.5}$, the mixing process is faster with one flamelet than with 20 flamelets leading to a stronger heat release and a higher pressure.

Also shown in Figure 6 is the pressure of a simulation with nine flamelets, which is identical with the pressure obtained with 20 flamelets except for the very early partially premixed phase. The resulting exhaust gas concentration for the pollutants NO_x and soot for these to cases only differed by less than 1%. Therefore, all following simulations were performed with nine flamelets. It is emphasized that none of the model constants in any model was changed to obtain the following results. Only the injection rates and fuel masses were prescribed corresponding to the measured ones.

Figures 8 and 9 compare the measured and simulated pressure traces. Again, it has to be noted that the measured pressure traces are disturbed by pipe oscillations as mentioned above. Therefore, these oscillations cannot be reproduced by the simulations. Apart from that they agree

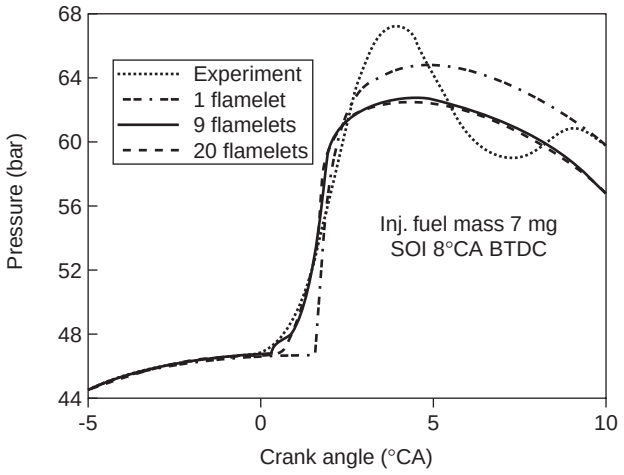

Figure 6

The influence of the number of flamelets on pressure.

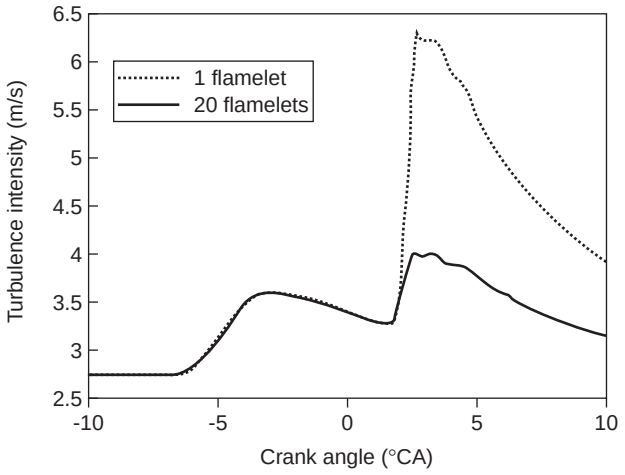

Figure 7

The influence of the number of flamelets on the cylinder averaged turbulence intensity.

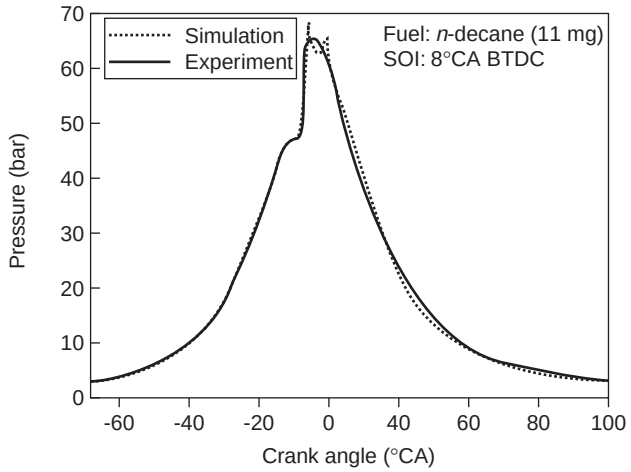

Figure 8

Measured and simulated cylinder pressures (*n*-decane).

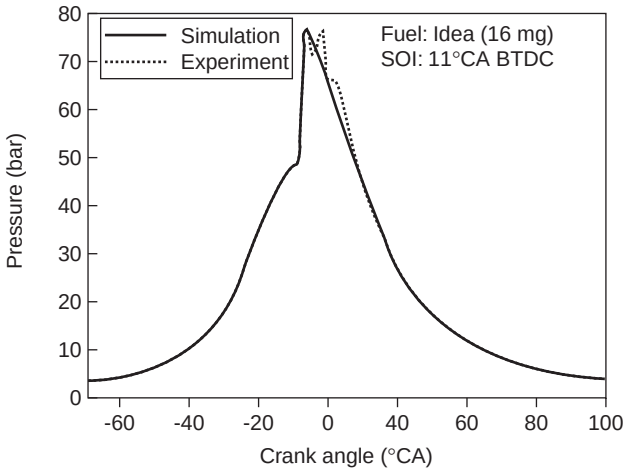

Figure 9

Measured and simulated cylinder pressures (Idea).

very well over the whole cycle for both cases. Especially the ignition delay time is predicted accurately. The ignition delay time of a homogeneous mixture of *n*-decane and air for an equivalent pressure and temperature and an equivalence ratio $\Phi = 2$ is approximately 0.4 ms, corresponding to 4.8° CA. The heat and radical production by chemical reactions is balanced by the diffusive transport, which is proportional to the local strain in the combustion chamber. Ignition occurs, when the chemical production exceeds the diffusive transport. Therefore, the ignition delay time is controlled by strain effects, which are represented by the scalar dissipation rate in the flamelets.

In Figure 10 the temporal evolution of the scalar dissipation rate conditioned at stoichiometric mixture χ_{st} for all nine flamelets and its cylinder averaged value is displayed. Shortly after start of injection χ_{st} starts to increase due to the evaporating fuel. Initially only one flamelet is needed, since the extension of the mixture field is small in the beginning, and only a small portion of the total fuel mass is injected yet. As the mixture field extends in the turbulent flow field the value for χ_{st} begins to vary locally from its mean value in the flamelet domain, which is the whole combustion chamber initially. When the variance becomes large, the flamelet domain is subdivided. Corresponding to the local level of χ_{st} one new domain contains all the regions, where st is lower than the former mean value of χ_{st} of the old domain, and vice versa. At approximately 7° CA BTDC this process occurs the first time. Both resulting flamelets start from the solution of the former single flamelet (temperature, species mass fractions), thereby inheriting the history of the old flamelet. But from this point they experience a different evolution of χ_{st} , because of there different paths through the turbulent flow field. This is represented by the two fine lines departing from the bold line with dots in Figure 10. The process of flamelet subdivision is then repeated until the maximum number of flamelets in the computation is reached. The average value of the scalar dissipation rate in the combustion chamber decreases due to the mixing process, which diminishes the variance of the mixture fraction field.

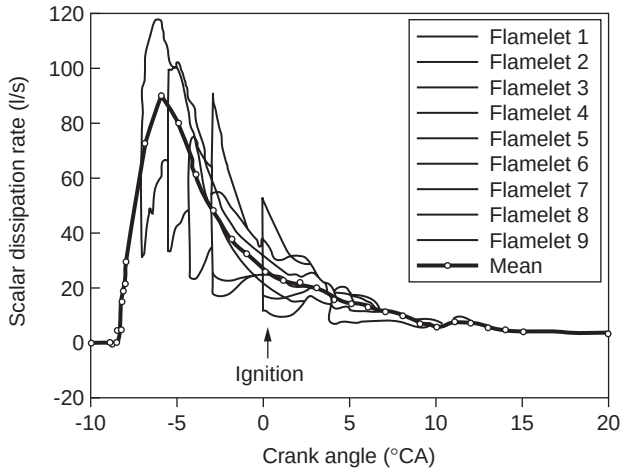

Figure 10

Scalar dissipation rates of the flamelets.

The effect of the different histories of the flamelets is shown in Figures 11 and 12. Three temperature profiles in mixture fraction space corresponding to flamelets 1, 4, and 8 are displayed at TDC, where ignition occurs and 1° CA ATDC. In Figures 11 and 12 the value of χ_{st} is lowest for flamelet 1 and highest for flamelet 8. The value of χ_{st} for flamelet 4 represents approximately the average value in the

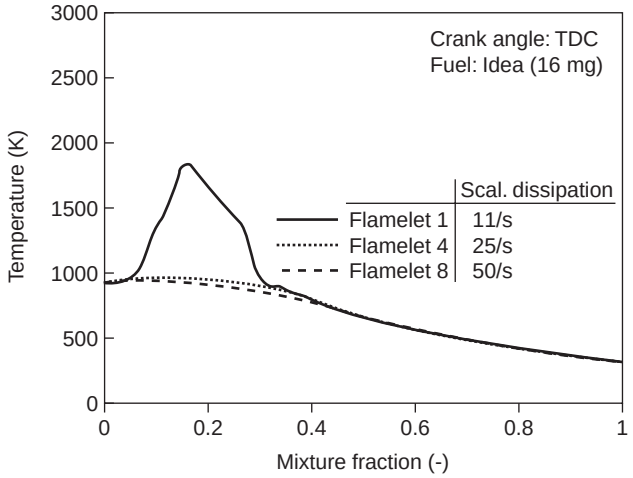

Figure 11

Temperature in different flamelets at TDC.

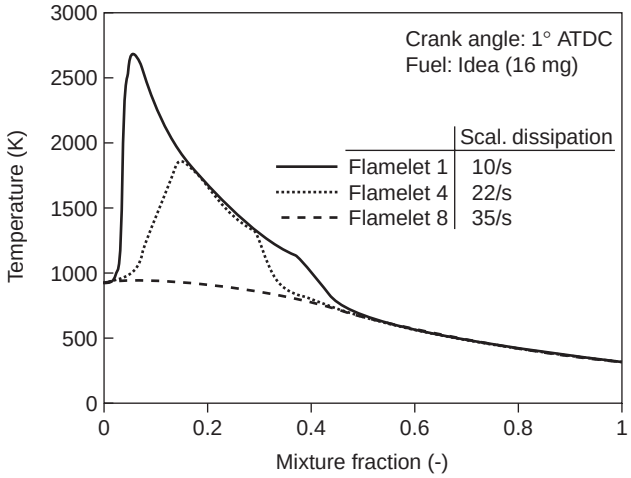

Figure 12

Temperature in different flamelets at 1° CA ATDC.

combustion chamber. The laminar diffusive transport in the flamelets is proportional to the value of χ_{st} . Therefore, a low χ_{st} is equivalent to a low heat loss and low radical transport from the reaction zone in the flamelets resulting in an earlier temperature rise. At TDC χ_{st} is low, long enough to allow flamelet 1 to ignite. Under Diesel engine conditions Ignition occurs in the rich part of the flame ($Z \approx 0.2$). The value of χ_{st} in flamelet 4 has reached a level, where ignition is possible, and hence, a moderate temperature rise can be observed compared to flamelet 8, where χ_{st} is still too high for any temperature rise in the flamelet.

One degree CA ATDC flamelet one is fully ignited and has reached its maximum temperature (Fig. 12). Flamelet 4 has ignited and is approximately in the state flamelet 1 was in 1° CA earlier. For flamelet 8 χ_{st} is still too high for a visible temperature rise. This process of consecutive ignition of the flamelets is responsible for the gradual pressure rise in the combustion chamber as displayed in Figure 6.

The exhaust gas values of the pollutants for the experiments and the simulations are shown in Table 1 and Figures 4 and 5. The agreement for NO_x and soot is very good. The maximum deviation for NO_x is lower than 7% and soot 4%, respectively.

TABLE 1

Pollutant concentrations in the exhaust gas

	NO_x (ppm)	Soot (mg/m^3)
Experiment *n*-decane	358	22
Simulation *n*-decane	383	21
Experiment Idea	541	244
Simulation Idea	581	235

Figure 13 shows the temporal evolution of the cylinder averaged mole fractions for NO_x, NO, and NO_2 for the simulation of 16 mg Idea-fuel. NO and NO_2 formation starts when ignition occurs. At 40° CA ATDC the NO_x level reaches its maximum. Approximately 13% NO_x are subsequently consumed. At the end of the combustion cycle NO_x consists of 85% NO and 15% NO_2.

The temporal evolution of the cylinder averaged soot mass concentrations is plotted in Figure 14. Soot formation starts with ignition. At 12° CA ATDC the soot mass concentration reaches a maximum value of approximately 19 g/m^3 (1210 mg/kg). This corresponds to 3.9% of the injected fuel mass. After that oxidation exceeds soot formation and the soot mass concentration decreases rapidly to a final value of 235 mg/m^3 (153 mg/kg). Hence, 87.5% of the maximum soot mass is oxidized again.

The effect of multiple flamelets on pollutant predictions is investigated in Figures 15 and 16. The NO and soot concentration profiles of the same flamelets (1, 4, and 8), which were considered during the ignition process above, are shown at 100° CA ATDC. The low value of χ_{st} of approximately 0.3 indicates that the mixture field is almost homogeneous. Although the levels of χ_{st} hardly differs for the different flamelets, significant deviations of the NO mass fractions in the flamelets are found. The relative difference between the maximum mass fraction of flamelets 1 and 8 is 30%, and 20% between flamelets 1 and 4, respectively. This is caused by two effects. Under Diesel engine conditions without exhaust gas recirculation the thermal NO formation path is predominant. It is strongly temperature dependent (increasing with increasing temperature). In a flamelet with a higher level of χ_{st} the temperature will be lower than in a flamelet with a low value of χ_{st}. Therefore, the NO formation by the thermal path will be lower in this flamelet, and since NO

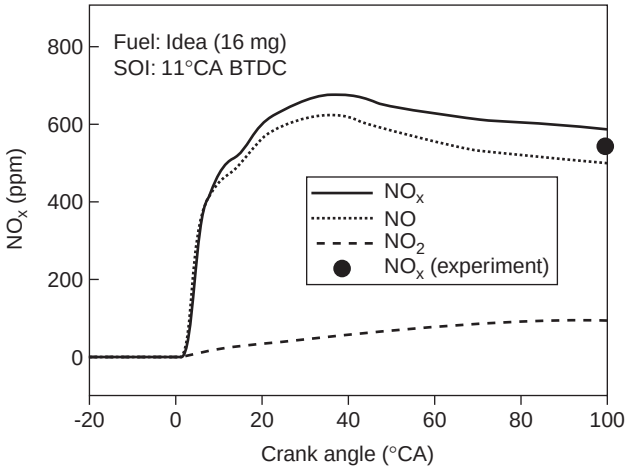

Figure 13

Cylinder averaged NO_x mole fractions.

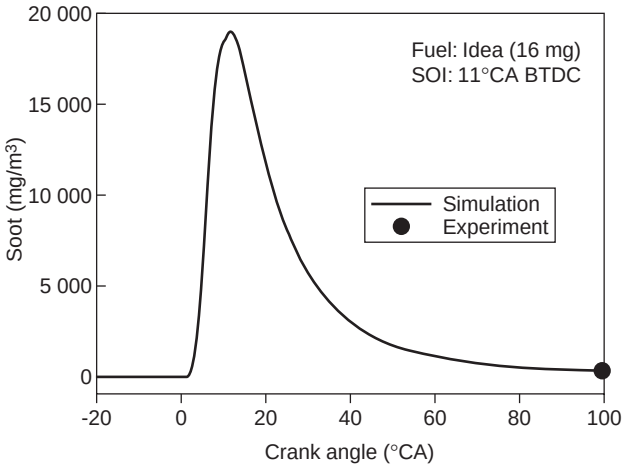

Figure 14

Cylinder averaged soot mass concentration.

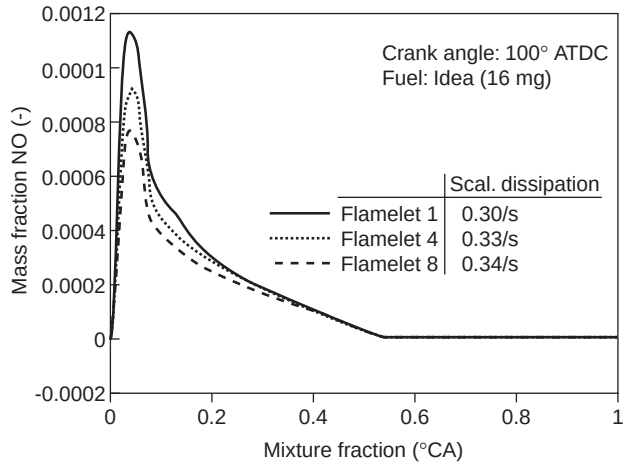

Figure 15

NO mass fractions in different flamelets at 100° CA ATDC.

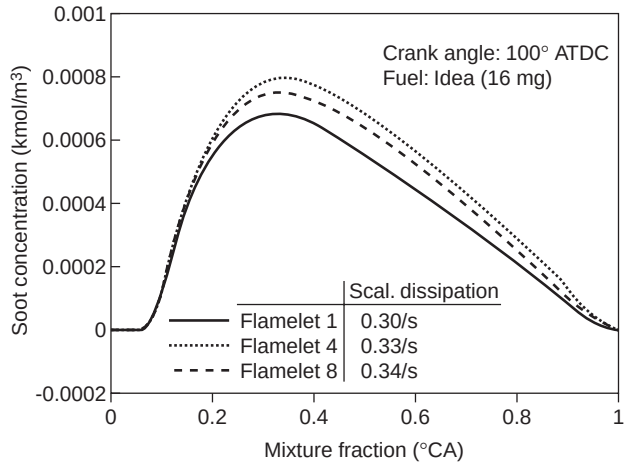

Figure 16

Soot concentration in different flamelets at 100° CA ATDC.

consumption is negligible to leading order this results in a lower overall NO level.

The second effect is that in a flamelet, which ignites earlier, more time is available in the high pressure and high temperature phase around TDC. Hence, more NO is produced.

The difference in the resulting soot concentrations (15%) is not as strong as for NO. For the soot concentrations both, formation and oxidation, are equally important. Both processes are temperature dependent.

Therefore, none of them can be neglected, and simple correlations to the ignition delay time and the temperature level in the flamelet are not found. This is reflected in Figure 16 where the soot concentration profile for flamelet 8 with the highest level of the scalar dissipation rate and the longest ignition delay time lies within the other two.

CONCLUSION

For successful modeling of Diesel engine combustion a reference fuel, which accounts for the many compounds of Diesel-fuel, is essential. Two of them, for which chemical reaction mechanisms have been developed, were compared to Diesel-fuel experimentally in a Volkswagen DI Diesel engine. The engine was fired with Diesel and the two reference fuels (*n*-decane, Idea-fuel) at different loads. The results show very good agreement between Diesel and Idea-fuel for ignition delay, heat release, and pollutant formation.

This agreement is explained by the physical (density, viscosity, etc.) and chemical (cetane number, aliphatic and aromatic compounds) similarity of both fuels.

Encouraged by this results simulations with the two reference fuels were performed applying the RIF model, which was recently extended for multiple flamelets.

First the influence of the number of flamelets used in the simulations was investigated. It was found that nine flamelets gave sufficiently accurate results for whole combustion process including pollutant formation.

Two simulations with *n*-decane (11 mg, SOI 8° CA BTDC) and Idea-fuel (16 mg, SOI 11° CA BTDC) were compared to the experimental data. All parameters and model constants except for the injection rates and masses were constant for the simulations. The agreement for the cylinder pressures and exhaust gas concentrations of the pollutants was excellent.

ACKNOWLEDGMENTS

This research was supported by the *European Commission* in the frame of the Joule III-Programme (JOF3-CT95-0003) and by the *Swedish National Board* for *Industrial and Technical Development Nutek* within the Diesel project and by *Bayerische Forschungsstiftung* (AZ: 177/96) in the project: “Potential neuartiger Einspritzverfahren zur Reduzierung von Rußund NO_x bei der dieselmotorischen Verbrennung”.

REFERENCES

1 Peters, N. (1984) Laminar Diffusion Flamelet Models in Non-Premixed Turbulent Combustion, Prog. *Energy Combust. Sci.*, 10, 319-339.

2 Pitsch, H., Wan, Y.P. and Peters, N. (1995) Numerical Investigation of Soot Formation and Oxidation Under Diesel Engine Conditions. *SAE Paper* 952357.

3 Pitsch, H., Barths, H. and Peters, N. (1996) Three-Dimensional Modeling of NO_x and Soot Formation in DI-Diesel Engines Using Detailed Chemistry Based on the Interactive Flamelet Approach. *SAE Paper* 962057.

4 Barths, H., Antoni, C. and Peters, N. (1998) Three-Dimensional Simulation of Pollutant Formation in a DI-Diesel Engine Using Multiple Interactive Flamelets. *SAE Paper* 982459.

5 Bray, K.N.C. and Peters, N. (1994) *Laminar Flamelets in Turbulent Flames, in Turbulent Reacting Flows,* Libby, P.A. and Williams, F.A. Eds, Academic Press, London.

6 Peters, N. (1987) Laminar Flamelet Concepts in Turbulent Combustion. *Twenty-First Symposium (International) on Combustion,* The Combustion Institute, Pittsburgh, 1231-1250.

7 Pitsch, H. and Peters, N. (1998) A Consistent Flamelet Formulation for Non-Premixed Combustion Considering Differential Diffusion Effects. *Combust. Flame,* **114**, 26-41.

8 McGuirk, J. and Jones, W.P. (1980) Computation of a Round Turbulent Jet Discharging into a Confined Cross Flow. *Turbulent Shear Flows,* 2, 233.

9 Pitsch, H., Chen, M. and Peters, N. (1998) Unsteady Flamelet Modeling of Turbulent Hydrogen/Air Diffusion Flames, accepted for presentation at *Twenty-Seventh Symposium (International) on Combustion,* The Combustion Institute, Pittsburgh.

10 Amsden, A.A., O'Rourke, P.J. and Butler, T.D. 1989) (Kiva-II: A Computer Program for Chemically Reactive Flows with Sprays. *Los Alamos National Laboratories,* LA-11560-MS.

11 Pitsch, H. and Peters, N. (1996) Reduced Kinetics of Multicomponent Fuels to Describe the Auto-Ignition, Flame Propagation and Post Flame Oxidation of Gasoline and Diesel Fuels. *Final Report, Idea Effect.*

12 Baulch, D.L., Cobos, C.J., Cox, R.A., Frank, P., Hayman, G., Just, Th., Kerr, J.A., Murrells, T., Pilling, MJ., Troe, J., Walker, R.W. and Warnatz, J. (1992) Evaluated Kinetic Data for Combustion Modeling. *J. Phys. Chem. Ref. Data,* **21**, 411-429.

13 Benson, S.W. (1981) *Prog. Energy Comb. Sci.,* 7, 125.

14 Chevalier, C., Louessard, P., Mu, C. and Warnatz, J. (1990) A Detailed Low-Temperature Reaction Mechanism of *n*-Heptane Auto-Ignition. *Int. Symp. on Diagnostics and Modeling of Combustion in Internal Engines Comodia 90,* Kyoto, The Japan Society of Mechanical Engineers.

15 Westbrook, C.K., Warnatz, J. and Pitz, W.J. (1988) A Detailed Chemical Kinetic Reaction Mechanism for the Oxidation of Iso-Octane and *n*-Heptane over an Extended Temperature Range and its Application to Analysis of Engine Knock. *Twenty-Second Symposium (International) on Combustion,* The Combustion Institute, Pittsburgh, 893-901.

16 Hewson, J.C. and Bollig, M. (1996) Reduced Mechanisms for NO_x Emissions from Hydrocarbon Diffusion Flames. *Twenty-Sixth Symposium (International) on Combustion,* The Combustion Institute, Pittsburgh, 2171-2180.

17 Mauss, F. (1997) Entwicklung eines Kinetischen Modells der Rußbildung mit Schneller Polymerisation. *PhD Thesis,* RWTH Aachen.

18 Frenklach, M. and Warnatz, J. (1987) Detailed Modeling of PAH Profiles in a Sooting Low-Pressure Acetylene Flame. *Combust. Sci. Technol.,* 51, 265.

19 Miller, J.A. and Melius, C.F. (1992) Kinetic and Thermo-dynamic Issues in the Formation of Aromatic Compounds in Flames of Aliphatic Fuels. *Combust. Flame,* **91**, 21-39.

20 Pitsch, H. (1997) Modellierung der Zund Schadstoffbildung bei der Dieselmotorischen Verbrennung mit Hilfe eines Interaktiven Flamelet-Modells. *PhD Thesis,* RWTH Aachen.

21 Frenklach, M. and Harris, S.J. (1987) Aerosol Dynamics Modeling Using the Method of Moments. *J. Coll. Interf. Sci.,* **118**, 1.

22 Arcoumanis, C. and Whitelaw, J.H. (1993) Experiments on Spray Development and Combustion in DI Diesel Engines. *Final Report, Idea.*

23 Bäcker, H., Hild, O. and Lepperhoff, G. (1995) Formation and Oxidation of Soot and Gaseous Pollutants Inside a Diesel Combustion Chamber Under the Influence of Exhaust Gas Recirculation. *Periodic Report,* 01/07/1995-31/12/1995, Idea Effect.

24 Hentschel, W. and Schindler, K.P. (1993) Experimental Investigation of Spray Formation and Combustion in a Real Diesel Engine. *Final Report,* Idea.

25 Hentschel, W. and Röpke, S. (1994) Influence of Exhaust Gas Recirculation on Diesel Combustion. *Periodic Report,* 01/01/1994-30/06/1994, *Idea Effect.*

26 Hentschel, W. and Röpke, S (1994) Influence of Exhaust Gas Recirculation on Diesel Combustion. *Periodic Report*, 01/07/1994-31/12/1994, *Idea Effect.*

27 Antoni, C. (1998) Untersuchung des Verbrennungsvorgangs im Direkteinspritzenden Dieselmotor mit Zyklusaufgel-Emissionsspektroskopie. *PhD Thesis*, RWTH Aachen.

28 Douch, M. (1998) Eine Parametrische Untersuchung zum Einflußdes Kraftstoffs auf die Schadstoffemissionen eines DI Dieselmotors. *Diploma Thesis*, RWTH Aachen.

29 Wolter, L. (1998) Aufbau und Inbetriebnahme eines Meßverfahrens zur Ermittlung des Einzpritzverlaufs von Dieselanlagen. *Diploma Thesis*, RWTH Aachen.

30 Strauss, T.S. and Volkswagen AG (1996) *Private Communication.*

31 Arcoumanis, C. and Jeong, K.S. (1991) Steady Flow Characterization of the Volkswagen 1.9 l Diesel Cylinder Head., *Technical Report* submitted to Volkswagen AG, Mechanical Engineering Dept., Imperial College of Science, Technologie and Medicine, London.

32 Barths, H. and Peters, N. (1998) Implication of Spray Modelling on the Prediction of Pollutant Formation in DI-Diesel Engines. *Proceedings of the Fourteenth International Conference on Liquid Atomization and Spray Systems* (ILASS Europe).

Final manuscript received in March 1999